International Journal of Naval Architecture and Ocean Engineering 12 (2020) 314–324

Contents lists available at ScienceDirect

International Journal of Naval Architecture and Ocean Engineering

journal homepage: http://www.journals.elsevier.com/international-journal-of-naval-architecture-and-ocean-engineering/

Experimental and numerical study of autopilot using Extended Kalman Filter trained neural networks for surface vessels

Yuanyuan Wang [a, b, *], Shuhong Chai [a], Hung Duc Nguyen [a]

[a] National Centre for Maritime Engineering and Hydrodynamics, Australian Maritime College, University of Tasmania, Launceston, TAS, 7250, Australia
[b] Research and Development Centre of Maritime Autonomous Surface Ship, iCloudNav, Zhuhai, Guangdong, 519000, China

ARTICLE INFO

Article history:
Received 9 March 2018
Received in revised form
6 November 2019
Accepted 11 November 2019
Available online 8 April 2020

Keywords:
Neural networks
Extended Kalman filter training
Free running experiment
Model scaled vessel

ABSTRACT

Due to the nonlinearity and environmental uncertainties, the design of the ship's steering controller is a long-term challenge. The purpose of this study is to design an intelligent autopilot based on Extended Kalman Filter (EKF) trained Radial Basis Function Neural Network (RBFNN) control algorithm. The newly developed free running model scaled surface vessel was employed to execute the motion control experiments. After describing the design of the EKF trained RBFNN autopilot, the performances of the proposed control system were investigated by conducting experiments using the physical model on lake and simulations using the corresponding mathematical model. The results demonstrate that the developed control system is feasible to be used for the ship's motion control in the presences of environmental disturbances. Moreover, in comparison with the Back-Propagation (BP) neural networks and Proportional-Derivative (PD) based control methods, the EKF RBFNN based control method shows better performance regarding course keeping and trajectory tracking.

1. Introduction

For the seagoing vessels, autopilots are widely utilised in various aspects and circumstances. The adoption of autopilot is of vital importance in reducing operating costs and human risks as it is helpful to liberate the productive forces of deck-officers. In addition, the feasible autopilot would enhance the vehicle's motion control reliability, especially for ships sailing in constrained waters like straits, coastal waters, and area of traffic separation scheme. It is also essential for the ship to accomplish special operations like placing cables and replenishment at sea. Moreover, the development of intelligent autopilot will speed up the applications of the unmanned surface vessels to perform survey, monitoring and data collection tasks.

Actually, the control of surface vessels remains a challenge because of the nonlinear hydrodynamic characteristics and underactuation. Considering the reliability and simplification, the conventional proportional-integrative-derivative (PID) controller has been extensively employed in designing autopilot. However, when the ship encounters complicated external disturbances and uncertainties, the control performance of the PID autopilot will be significantly affected even using the gain scheduling method (Tannuri et al., 2010). This is the reason why manual steering is required when the ship is sailing on severe seas. In recent decades, due to the development of the modern control theory, various control strategies including genetic algorithm (Naeem et al., 2005), back-stepping control (Dong et al., 2015), sliding mode control (Wang et al., 2017a, 2018a), finite-time uncertainty observer based control (Wang et al., 2018b) and fuzzy logic control (Rigatos and Tzafestas, 2006) have been investigated to enhance the capability of ship's autopilot. Although the benefits of the above-mentioned control strategies are attractive, some limitations need to be addressed, such as the time consumption of generation propagation, the unexpected tracking error generated from the previous error conditions, and the difficulties in formulating the fuzzy control rules (Sun et al., 2014).

Prompted by the booming of computing technology, the neural network based control became applicable in engineering practice. Owing to the competent capability in approximating, neural network control algorithms have been employed to design the autopilot (Dai et al., 2012; Wang and Er, 2015; Wu et al., 2012; Wang

* Corresponding author. National Centre for Maritime Engineering and Hydrodynamics, Australian Maritime College, University of Tasmania, Launceston, TAS, 7250, Australia.
E-mail addresses: Yuanyuan.Wang@utas.edu.au (Y. Wang), Shuhong.Chai@utas.edu.au (S. Chai), H.D.Nguyen@utas.edu.au (H.D. Nguyen).
Peer review under responsibility of Society of Naval Architects of Korea.

https://doi.org/10.1016/j.ijnaoe.2019.11.004

et al., 2018c). In comparison with another multilayer feed-forward neural networks, the Radial Basis Function Neural Network (RBFNN) is feasible to approximate unknown functions without completing prior information (Park and Sandberg, 1991). Also, the RBFNN has simple architecture and good generalisation capability, which is beneficial to avoid unnecessary and lengthy calculation (Liu, 2013). Thus, RBFNN is employed in this study.

It is known that the training algorithm is essential to the design of the neural network controller. Besides the extensively utilised BP training algorithm, other training methods including supervised gradient descent and back-stepping have been investigated (Yahui et al., 2004). Although these algorithms have been proved to be effective in some applications, the relevant limitations cannot be discarded: firstly, the calculation of dynamic derivatives regarding the relative weights is computationally expensive (Sum et al., 1999); secondly, the training with gradient descent methods tends to be slow and poor in approaching satisfactory results (Trebatick, 2005). The attention to address these flaws became the motivation for investigating more efficient network training algorithm.

From another point of view, the process of neural networks training can be considered as a parameter estimation problem. The Kalman Filter (KF) or its variant are alternatives with the capability of providing online approaches to optimise the weights of the networks (Sanchez et al., 2008). Among them, the Extended Kalman Filter (EKF) algorithm can provide a mechanism in which the weights can be updated immediately (Purushothaman, 2010). The obvious difference between widely adopted BP and EKF training method is that the former method only updates the weights, whereas the EKF algorithm updates weights as well as approximation error covariance. In addition, contrary to some higher-order training methods, the EKF based training algorithm for networks do not require batch processing, making it less computationally expensive in recursive usage. It is indicated that the converge speed is improved and the number of design parameters is decreased when the EKF training algorithm is applied to train neural networks (Yang et al., 2007).

Based on the above-mentioned motivations, the EKF is adopted as the training method of RBFNN based controller for ships sailing with the environmental disturbances and observer uncertainties. The main objectives of this study are: 1) to propose the EKF RBFNN based control system to control the motion of surface vessel; 2) to introduce the configurations of the newly developed free running model scaled ship (FRMSS), which is constructed by the mechatronic hardware and low-cost sensors; 3) to experimentally and numerically conduct the validations of the proposed autopilot; 4) to analyse the control performance of the developed autopilot through the comparison with that of BP RBFNN and PD based systems.

The paper is organised as follows: Section 2 introduces the mechatronic elements of the employed FRMSS and the relevant motion equations. The design of EKF RBFNN based autopilot is presented in the following section with regard to the ship's trajectory tracking. After that, numerical and experimental validations are presented to verify the capability of the proposed controller. The corresponding conclusions are drawn in the last section.

2. The free running model scaled ship and dynamic model of motions

To investigate the proposed control system in a realistic engineering environment, the FRMSS was employed to conduct the numerical study and closed-loop experiments taking on the Trevallyn Lake in Launceston (Tasmania, Australia). The physical model is a 1:100 scaled replica of the 'M/V Nedlloyd: Hoorn' (the main characteristics are outlined in Table 1), whose hydrodynamic design and loading condition follow the properties of the full scale ship. The geometric, kinetic and dynamic similarity principles were preserved to guarantee that experiments results can be further referred to real objects (Morawski and Pomirski, 1998). In this section, the configurations of the ship and the four Degree of Freedom (DOF) motion equations are presented.

2.1. Mechatronic of the free running model scaled ship

The mechanical and electronic elements of the ship were installed in the Control Lab of Australian Maritime College. The configurations of the physical model are shown in Fig. 1 with the following five sub-systems:

1). Power supply system: 6 lead acid batteries are carried on the ship to provide electricity to the electronic devices and actuators. 2). Actuators system: Twin propellers are driven by two independent Brushless Direct Current (BLDC) motors controlled by two sets of Escon 50/5 amplifiers; the deflection of the rudder is determined by a medium speed servo motor driven by the pulse signal. 3). Embedded computer platform: The device myRIO, produced by National Instrument, is utilised as the embedded computer and Real-Time I/O platform. It features a 667 MHz dual-core programmable processor and a customizable Xilinx FPGA, incorporating with onboard memory and built-in WIFI module, to allow the users to deploy and run LabVIEW program remotely. Various data acquisition card ports are used to support the connections of SPI, PWM and I^2C. 4). Measurement system: The measurements are accomplished by using the sensors, including digital compass, gyroscope and accelerometer. The measured data are processed and logged in myRIO for further analysis. 5) Host computer: Host computer installed the LabVIEW is used to deploy the program and control the FRMSS remotely.

2.2. Motion equations of the surface ship

The motions of the ship contain three components: the position and orientation vector $\boldsymbol{\eta}$ defined in eartg-fixed coordinate, the linear and angular velocity vector $\boldsymbol{\nu}$ as well as the force and moment vector $\boldsymbol{\tau}$ defined in body-fixed coordinate. The relevant items to describe Hoorn's motion are illustrated in Fig. 2.

Normally, the three DOF mathematical model is sufficient to describe the surface vessel's motion. However, the experimental reading of the yaw rate transformed from the body-fixed coordinate to earth-fixed coordinate is influenced by huge roll motion. Thus, the ship's four DOF dynamic model is employed (Fossen, 1994) as Eq. (1):

$$\begin{cases} (m+m_x)\dot{u} - (m+m_y)vr = X \\ (m+m_y)\dot{v} + (m+m_x)ur + m_y\alpha_y\dot{r} - m_y l_y\dot{p} = Y \\ (I_x+J_x)\dot{p} - m_y l_y\dot{v} - m_x l_x ur + W\overline{H}\phi = K \\ (I_z+J_z)\dot{r} + m_y\alpha_y\dot{v} = N \end{cases} \tag{1}$$

where the involved items are outlined in Table 2.

Table 1
Main characteristics of the full scaled and model scaled 'Hoorn'.

Items	Values	
	Full Scale Vessel	Model Scaled Vessel
Length between perpendiculars (L)	247 m	2470 mm
Breadth (B)	32 m	320 mm
Draft (D)	12 m	120 mm
Mass (m)	64,000 T	63.4 kg
Metacentric height ($\overline{H}$)	0.875 m	8.75 mm

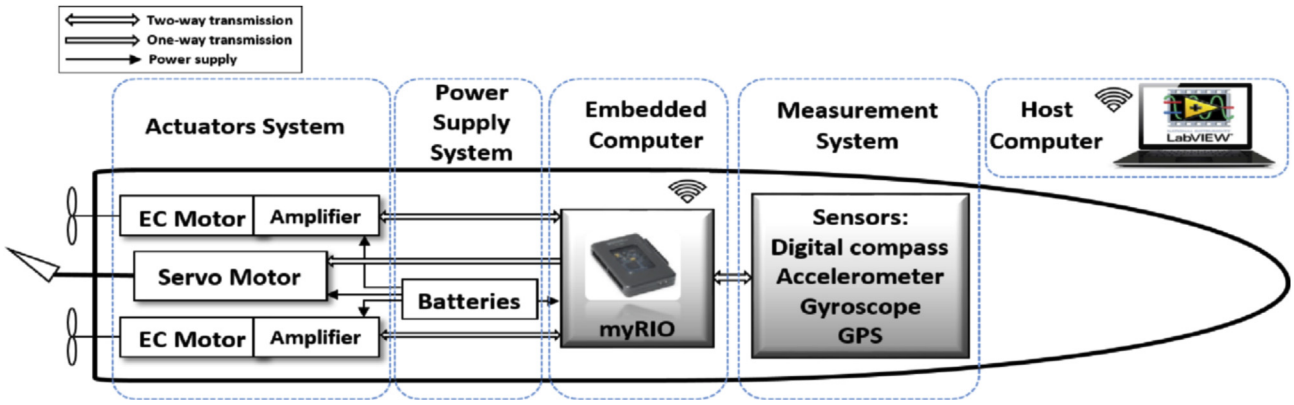

Fig. 1. The configurations of the free running model scaled 'Hoorn'.

The forces and moments in four DOF can be represented as Eq. (2)

$$[X_E \quad Y_E \quad K_E \quad N_E] = m[\overline{a_1} \quad \overline{a_2} \quad L\overline{a_3} \quad L\overline{a_4}]S$$

$$\begin{bmatrix} X \\ Y \\ K \\ N \end{bmatrix} = \begin{bmatrix} X_{uu}u^2 + (1-t_P)T_P + X_{vr}vr + X_{vv}v^2 + X_{rr}r^2 + X_{\phi\phi}\phi^2 + (1-t_R)F_N \sin\delta \; ; \\ Y_v v + Y_r r + Y_{vvv}v^3 + Y_{vvr}v^2 r + Y_{vrr}vr^2 + Y_{vv\phi}v^2\phi + (1+a_H)F_N \cos\delta \; ; \\ K_v v + K_r r + K_p p + K_{vvv}v^3 + K_{vvr}v^2 r + K_{vrr}vr^2 + K_{vv\phi}v^2\phi + K_{rr\phi}r^2\phi \\ +(1+a_H)z_R F_N \cos\delta \; ; \\ N_v v + N_r r + N_p p + N_{vvv}v^3 + N_{rrr}r^3 + N_{vvr}v^2 r + N_{vrr}vr^2 + N_{vv\phi}v^2\phi \\ +N_{v\phi\phi}v\phi^2 + N_{rr\phi}r^2\phi + N_{r\phi\phi}r\phi^2 + (x_R + a_H x_H)F_N \cos\delta; \end{bmatrix} \tag{2}$$

where T_P is the propeller thrust force and F_N is the rudder force, which were identified by the captive test; δ is the rudder angle; $X_{\cdot}$, $Y_{\cdot}$, $K_{\cdot}$ and $N_{\cdot}$ with subscripts are the corresponding hydrodynamic coefficients identified from the experimental method (Wang et al., 2017b); a_H, t_P and t_R are the parameters for describing the interference extents between the hydrodynamic forces and moments acting on hull, propeller and rudder; x_R, x_H and z_R are the dimension parameters related to the ship's centre of gravity.

To describe the environmental disturbance acting on the ship, the modified Pierson-Moskowitz (PM) wave spectrum model recommended by ITTC and outlined in Fang and Lee (2016) were utilised and inserted into the right hands of the motion equations by using Eq. (3)

$$\ddot{S} + 2\xi w_e \dot{S} + w_e^2 S = 2\xi w_e \delta_w w_G \tag{3}$$

where $\bullet_E$ are the forces and moments of the waves, four $\overline{a}$ with subscripts represent the environmental impact parameters in every DOF, which were obtained by the experimental method in model test basin, L is the length of the ship, S is the wave model in time domain (Sgobbo and Parsons, 1999), $w_e = w_w - \frac{w_w^2}{g}Ucos\beta_w$ is the encounter wave frequency with speed at U and encounter angle β_w, w_w is the wave frequency, g is the gravity coefficient, ξ is the damping coefficient, δ_w is the wave intensity, and w_G is a zero-mean Gaussian white noise process used for generating the transfer function.

Combining the forces and moments of environmental disturbances, the equations of ship's motion can be written into the form of the ordinary differential equation (ODE) as Eq. (4)

$$\begin{bmatrix} \dot{u} \\ \dot{v} \\ \dot{r} \\ \dot{p} \\ \dot{\psi} \\ \dot{\phi} \end{bmatrix} = \begin{bmatrix} [X + X_E + (m+m_y)vr]/m_{11} \\ -[m_{33}m_{44}(Y + Y_E - (m+m_x)ur) + m_{32}m_{44}(K + K_E + m_x l_x ur - W\overline{H}\phi) + m_{42}m_{33}(N + N_E)]/m_a \\ \left[m_{42}m_{33}(Y + Y_E - (m+m_x)ur) + m_{32}m_{42}(K + K_E + m_x l_x ur - W\overline{H}\phi) + \left(m_{22}m_{33} - m_{32}^2\right)(N + N_E)\right]/m_a \\ \left[-m_{32}m_{44}(Y + Y_E - (m+m_x)ur) + \left(m_{22}m_{44} - m_{32}^2\right)(K + K_E + m_x l_x ur - W\overline{H}\phi) + m_{32}m_{42}(N + N_E)\right]/m_a \\ rcos\phi \\ p \end{bmatrix} \tag{4}$$

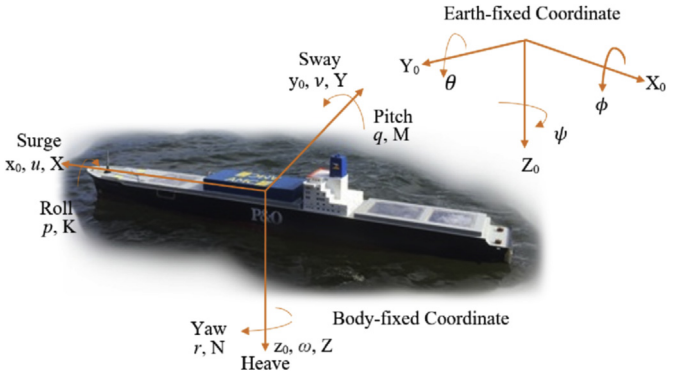

Fig. 2. The motion items of the surface vessel in Body-fixed Coordinate and Earth-fixed Coordinate.

Table 2
The items to describe the ship's four DOF motions.

Items		Meaning
$\overline{H}$		Metacentric heights
I_x, I_z		Inertia moments about x-axis and z-axis
J_x, J_z		Added inertia moments about x-axis and z-axis
l_x, l_y		Centres of m_x and m_y about z- axis
m, W		Mass and weights of the ship
m_x, m_y		Added masses about x-axis and z-axis
τ	X, Y	Forces in terms of surge and sway
	K, N	Moments in terms of yaw and roll
ν	p, r	Roll and yaw rate
	u, v	Surge and sway velocity
η	x, y	Position of the ship
	ϕ, ψ	Roll and yaw angle
α_y		Centre of m_y about x -axis

with $m_{11} = (m+m_x)$, $m_{22} = (m+m_y)$, $m_{32} = -m_y l_y$, $m_{42} = -m_y \alpha_y$, $m_{33} = (I_x + J_x)$, $m_{44} = (I_z + J_z)$, $m_a = m_{22}m_{33}m_{44} - m_{32}^2 m_{44} - m_{42}^2 m_{33}$. When the ODE solver is selected, the dynamic changes of the ship's attitude (i.e. $[u\ v\ r\ p\ \psi\ \phi]^T$) can be represented and described. More details about the specified values of manoeuvring and hydrodynamic parameters in four degrees of freedom (DOF) motion equations can be seen in Appendix.

3. EKF trained RBFNN autopilot design

In this section, the RBFNN based autopilot is proposed for the surface vessel. The main advantage of using RBFNN for controller design is that it is not necessary to know the accurate model of the ship in practical applications, even in the presence of unknown uncertainties. Although the BP methods work well in training neural networks, the convergence capability still needs to be risen because the gradient is calculated for the error surface defined by instant states but not the ensemble sates. In Ruck (1990), the BP training method was explained as the degenerate form of EKF training method mathematically. In this study, the utilisation of EKF training algorithm, which can be interpreted as the application of using EKF for parameters estimation, enables the RBFNN based controller to address the vessel's dynamics with external disturbances.

In this study, the RBFNN with three layers (namely, input layer, hidden layer and output layer) was employed. Particularly, the control law $\hat{u}_c$ estimated by the EKF RBFNN for the system can be expressed by the following equations as Eq. (5)

$$\begin{cases} z = \left[\chi_a \quad \dot{\chi}_a \lambda e + \dot{e}\dfrac{\lambda e + \dot{e}}{\varepsilon}\lambda e - \ddot{\chi}_d\right] \\ h(\boldsymbol{z})_i = exp\left(-\dfrac{\|\boldsymbol{z} - \boldsymbol{c_i^2}\|}{2b^2}\right) \\ \hat{u}_c(\boldsymbol{z}) = \dfrac{1}{\beta}\sum_{i=1}^{j}\hat{w}_i^T h(\boldsymbol{z})_i = \dfrac{1}{\beta}\left[\hat{w}_1 h\left(\boldsymbol{z}\right)_1 + \hat{w}_2 h\left(\boldsymbol{z}\right)_2 + \ldots + \hat{w}_j h\left(\boldsymbol{z}\right)_j\right] \end{cases} \tag{5}$$

where $\boldsymbol{z}$ is the input matrix of the RBFNN based controller, χ_a is the actual state of the plant being controlled, χ_d is the desired state, $e = \chi_d - \chi_a$ is the deviation between the actual and desired state, λ and ε are the design parameters to balance the converge speed and approximation accuracy within the range [0 1], more details about the construction of the input matrix as well as the parameters can be seen in Ge et al. (2013); in this study, the states being controlled are the yaw angle in vector $\boldsymbol{\eta}$ and the velocity in vector $\boldsymbol{\nu}$ which are described in section 2.2; $h(\boldsymbol{z})_i$ is the Radial Basis Function which works as the activation function of each neuron, $\mathbf{c}$ is the centre of the activation function and b is the width of the activation function, β is the limitation item of control law to constrain the action of actuators within practical value which is normally determined empirically, j is the total number of neuron nodes in the hidden layer, $\hat{w}$ is the estimated weights updated by EKF algorithm in this study, which can be executed in the following steps.

- Step Initialization

  Initialize with (shown as Eqs. (6) and (7)):

$$\text{Initial weights } \hat{\boldsymbol{w}}_0 = E[\boldsymbol{w}_0] \tag{6}$$

$$\text{Initial covariance } \boldsymbol{P}_0 = E\left[(\boldsymbol{w}_0 - \hat{\boldsymbol{w}}_0)(\boldsymbol{w}_0 - \hat{\boldsymbol{w}}_0)^T\right] \tag{7}$$

  Process noises covariance. $\boldsymbol{Q}$
  Observation noises covariance. $\boldsymbol{R}$

- Step 1: Prediction transformation (shown as Eqs. (8) and (9)):

$$\text{Predicted weights: } \hat{\boldsymbol{w}}_{k|k-1} = \hat{\boldsymbol{w}}_{k-1} \tag{8}$$

Predicted covariance: $\boldsymbol{P}_{k|k-1} = \boldsymbol{P}_{k-1}$ (9)

- Step 2: Observation transformation (shown as Eqs. (10)–(12)):

Jacobin aatrix: $\boldsymbol{H}_k = \frac{\partial \widehat{u}_c}{\partial \widehat{\boldsymbol{w}}_{k-1}}|_{\widehat{\boldsymbol{w}}_{k|k-1}} = \left[exp\left(-\frac{\|\boldsymbol{z} - \boldsymbol{c}_1^2\|}{2b^2} \right) \quad \cdots \quad exp\left(-\frac{\|\boldsymbol{z} - \boldsymbol{c}_j^2\|}{2b^2} \right) \right]_k$ (10)

Measurement covariance 1: $\boldsymbol{P}_{\boldsymbol{k}}^{\boldsymbol{1}} = \boldsymbol{H}_k \boldsymbol{P}_{k|k-1} \boldsymbol{H}_{\boldsymbol{k}}^{\boldsymbol{T}}$ (11)

Measurement covariance 2: $\boldsymbol{P}_{\boldsymbol{k}}^{\boldsymbol{2}} = \boldsymbol{P}_{k|k-1} \boldsymbol{H}_{\boldsymbol{k}}^{\boldsymbol{T}}$ (12)

- Step 3: Weights calculation and update (shown as Eqs. (13)–(15)):

Kalman gain $\boldsymbol{K}_k = \boldsymbol{P}_{\boldsymbol{k}}^{\boldsymbol{2}} \Big/ \left(\boldsymbol{P}_{\boldsymbol{k}}^{\boldsymbol{1}} + \boldsymbol{R} \right)$ (13)

Weights $\widehat{\boldsymbol{w}}_k = \widehat{\boldsymbol{w}}_{k|k-1} + \boldsymbol{K}_k s$ (14)

Approximate error covariance $\boldsymbol{P}_{k+1} = \boldsymbol{P}_{k|k-1} - \boldsymbol{K}_k \boldsymbol{H}_{\boldsymbol{k}}^{\boldsymbol{T}} \boldsymbol{P}_k + \boldsymbol{Q}$ (15)

where $\boldsymbol{K}_k$ is Kalman gain matrix for weights training in the k-th iteration, $\boldsymbol{P}_k$ is the approximate error covariance matrix, $\widehat{\boldsymbol{w}}_k$ is the estimated weights, $\boldsymbol{H}_k$ is the Jacobian matrix which is derived from the partial derivatives of the output of the system in relation to the weights and equals to the matrix of neural activation functions, $s = e + \dot{e}$ is the augmented error item containing the deviation and derivative of deviation between the desired and actual state, $\boldsymbol{R}$ and $\boldsymbol{Q}$ are the observation noise and artificial process noise covariance which is beneficial to avoid numerical divergence.

The architecture of the EKF RBFNN based autopilot can be achieved by using the above-mentioned control algorithm. The velocity of the ship is controlled by changing the shaft speed of the propellers to maintain the ship sailing with desired velocity. The yaw motion of the ship is controlled by the fluctuations of the rudder, whose control law is calculated by using the desired angle ψ_d and the actual yaw angle ψ as the elements of the RBFNN input matrix. Specifically, the function of route tracking is fulfilled by getting the dynamic desired yaw angle calculated by the Enclosure-Based-Steering Line-of-Sight (EBS LOS) guidance method incorporated with actual position and pre-set waypoints, while the function of controlling yaw angle is fulfilled by controlling the actual yaw angle to converge the desired yaw angle. As a result, the actuators will ensure the ship tracking the desired position and velocity reference signal (see in Fig. 3).

The dynamic desired course angle ψ_d to track the route can be calculated as Eq. (16):

$$\psi_d = \begin{cases} \dfrac{\pi}{2} & |x_{los} - x_c| = 0,\ y_{los} - y_c > 0 \\ \dfrac{3\pi}{2} & |x_{los} - x_c| = 0,\ y_{los} - y_c < 0 \\ tan^{-1}\left(\dfrac{y_{los} - y_c}{x_{los} - x_c} \right) & others \end{cases} \tag{16}$$

where (x_c, y_c) is the current position, $(x_{los}\ ,\ y_{los})$ is the position of EBS LOS point, which is calculated by using the previous pre-set waypoint, the following pre-set waypoint and orientation of the pre-determined trajectory, more details can be seen in Fossen (2011).

In order to evaluate the capability of the control system, the cost functions of yaw error C_Y and rudder deflection C_R were employed in this study as follows (Burns, 1995) in Eq. (17):

$$C_Y = \sum_{i=0}^{n} (\Delta\psi_i)^2;\ C_R = \sum_{i=0}^{n} \delta_i^2 \tag{17}$$

where n is the total amount of the iterations, $\Delta\psi_i$ and δ_i represent the yaw angle error and rudder deflection of the i -th iteration respectively.

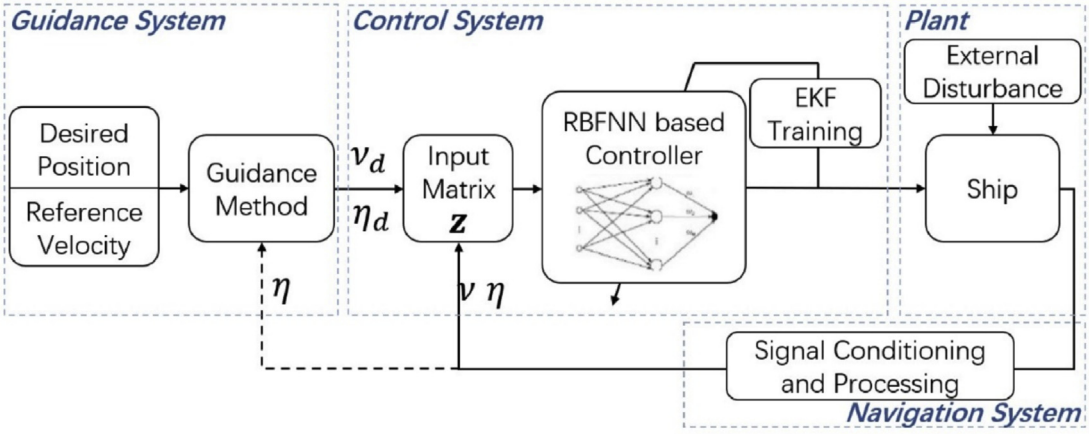

Fig. 3. Illustration of the EKF RBFNN based control system for the ship with external disturbance.

4. Numerical results and discussion

To validate the capabilities of the proposed EKF RBFNN based autopilot and promote parameters tunning process, the numerical studies are conducted by using the four DOF mathematical model of 'Hoorn' shown in Tables 5 and 6 (Wang et al., 2017b). The inputs of the mathematical model contain the rudder angle, shaft speed of the propellers and the external disturbances. The maximum rudder deflection was limited within ± 15 *degrees*, while the shaft speed was constrained within ± 1000 *rpm* to avoid unreasonable acceleration and deceleration. The external disturbance generated from random waves was adopted in the ship's motion equations, and the water depth was assumed to be infinite to disregard shallow water effects and band effects. The Bogacki-Shampine method was used to solve the ODE of the ship's motion responses in time series, including the velocity of surge, sway, yaw and roll, the angle of yaw and roll, the ship's position and the rudder angle. The parameters of the RBFNN based controller were set at $\varepsilon = 0.5$ and $\lambda = 4$, while the parameters involved the EKF training algorithm were $\boldsymbol{R} = \boldsymbol{I}_1$ and $\boldsymbol{Q} = 0.1 \times \boldsymbol{I}_9$. The environmental impact parameter vector is adopted as $\overline{\boldsymbol{a}} = [0.62\ 6.53\ 0.137\ 0.165]^T$ with equivalent sea state 4. In order to verify the performance of the proposed control system, the BP RBFNN based controller and PD based controller developed in Wang et al. (2015) were employed for comparison.

In the first scenario, the trajectory was planned from the initial waypoint at (0, 0) to the following waypoint (−200, −200) before heading to (−360, −800). The reference velocity was required to increase from the initial value at 0.5 m/s to the desired value at 1.38 m/s. In order to avoid the mis-controlling, the preliminary simulation was conducted by using the weights in Ge et al. (2013) to train the controller to handle the ship's motion control and get suitable initial weights matrix. In the following iterations, the

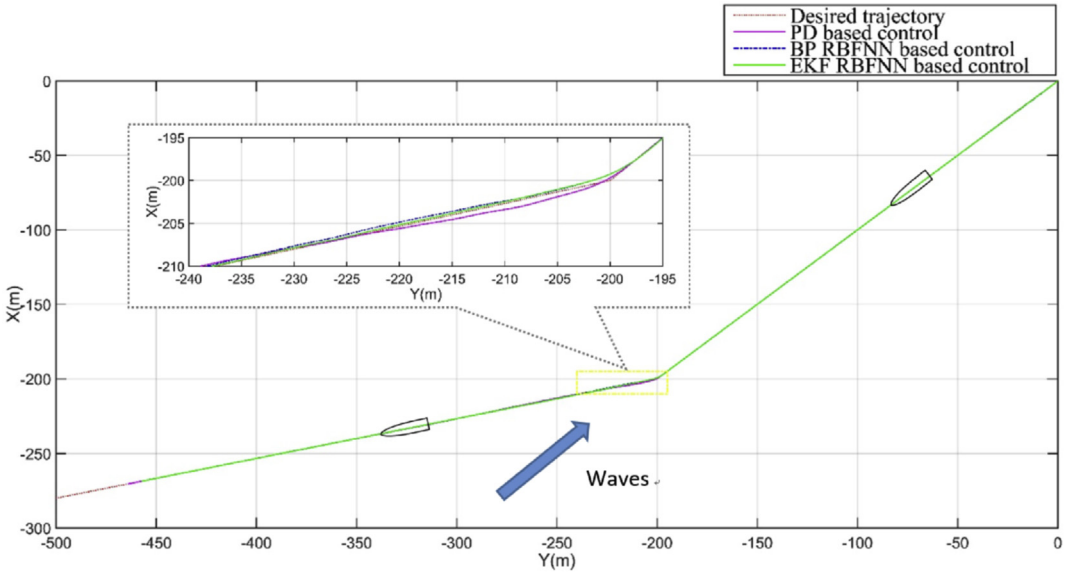

Fig. 4. Trajectory tracking of ship controlled by EKF RBFNN, BP RBFNN and PID based controller.

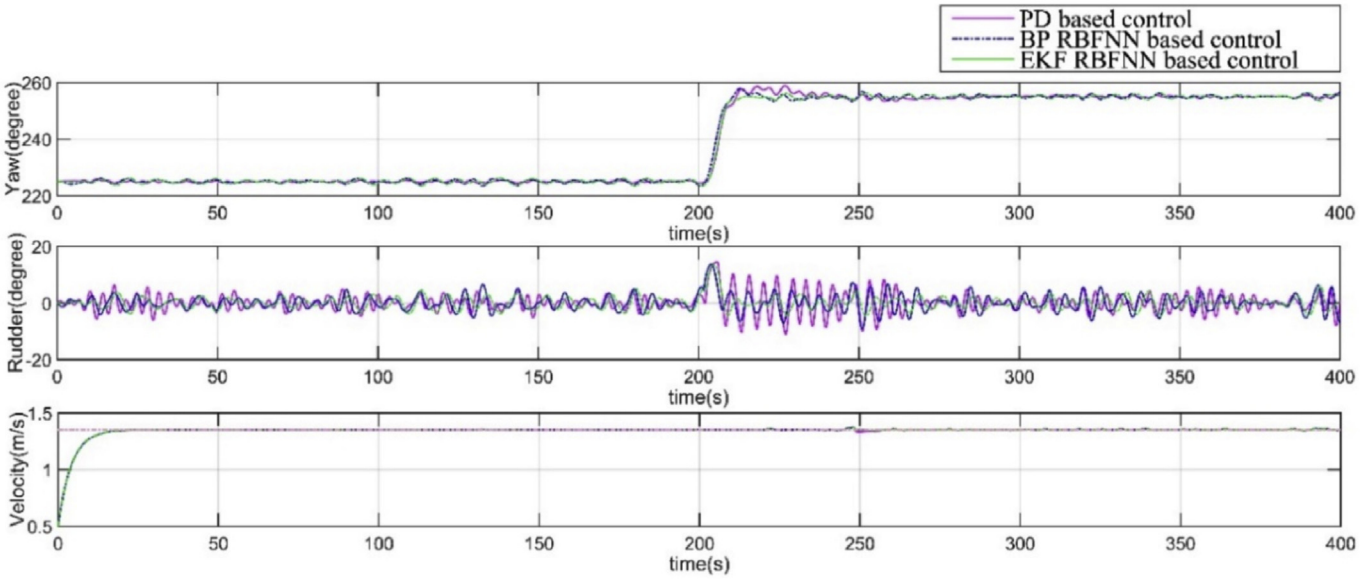

Fig. 5. The ship responses under the control of EKF RBFNN, BP RBFNN and PID controller based on the designed trajectory.

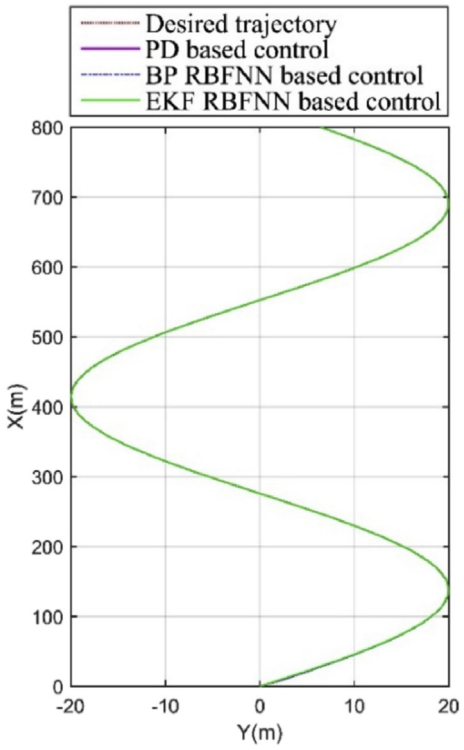

Fig. 6. Trajectory tracking of ship controlled by EKF RBFNN, BP RBFNN and PID based controller.

weights were trained online to make the plant converge to the desired state. The "convergent weights" were obtained in the stable stage with the weights varied within small range, which means the weights have adapted to the ship's inherent characteristics (Fang et al., 2010). Then, the "convergent weights" were selected as the initial base in the simulation validations. The following results show that, by using this strategy, the ship converges to the desired state with fast speed and small deviation even in the initial phase. The trajectories and the motion responses of the ship advancing according to the pre-set waypoints are shown in Fig. 4 and Fig. 5. It can be seen that, on the first track segment with waves on the head sea, the EKF RBFNN, BP RBFNN and PD based control system are well tuned and capable of maintaining the sailing position of the ship. When the third waypoint was selected for the guidance, the orientation of the pre-set track changed to 255° with waves on the bow sea, which led to the increase of the environmental disturbance acting on the ship. In order to counteract the changed disturbance, the PD based control system performed large rudder actions with high frequency. The EKF RBFNN based controller is superior to other two controllers in counteracting the increased external forces and moments using smooth rudder actions. It is noticeable that the settling speed of using EKF RBFNN based controller is also quicker than that of the BP RBFNN based controller. This can be attributed to the converging speed of the proposed training algorithm.

The same conclusion also can be drawn from the second scenario, in which the reference sinusoidal trajectory with amplitude at 20 m was adopted. The reference velocity was required to increase from the initial value at 1.0 m/s to the desired value at 1.38 m/s. Overall, Fig. 6 and Fig. 7 illustrate that the EKF RBFNN based control system is competent in trajectory tracking through reasonable actions of actuators. Based on the above-mentioned scenarios, the robustness of the proposed EKF RBFNN control system has been verified. In comparison with the BP trained RBFNN control system and PD based control system, the priorities of the EKF RBFNN based autopilot consists of the effective rudder actions and short settling time in coping with dynamical changes.

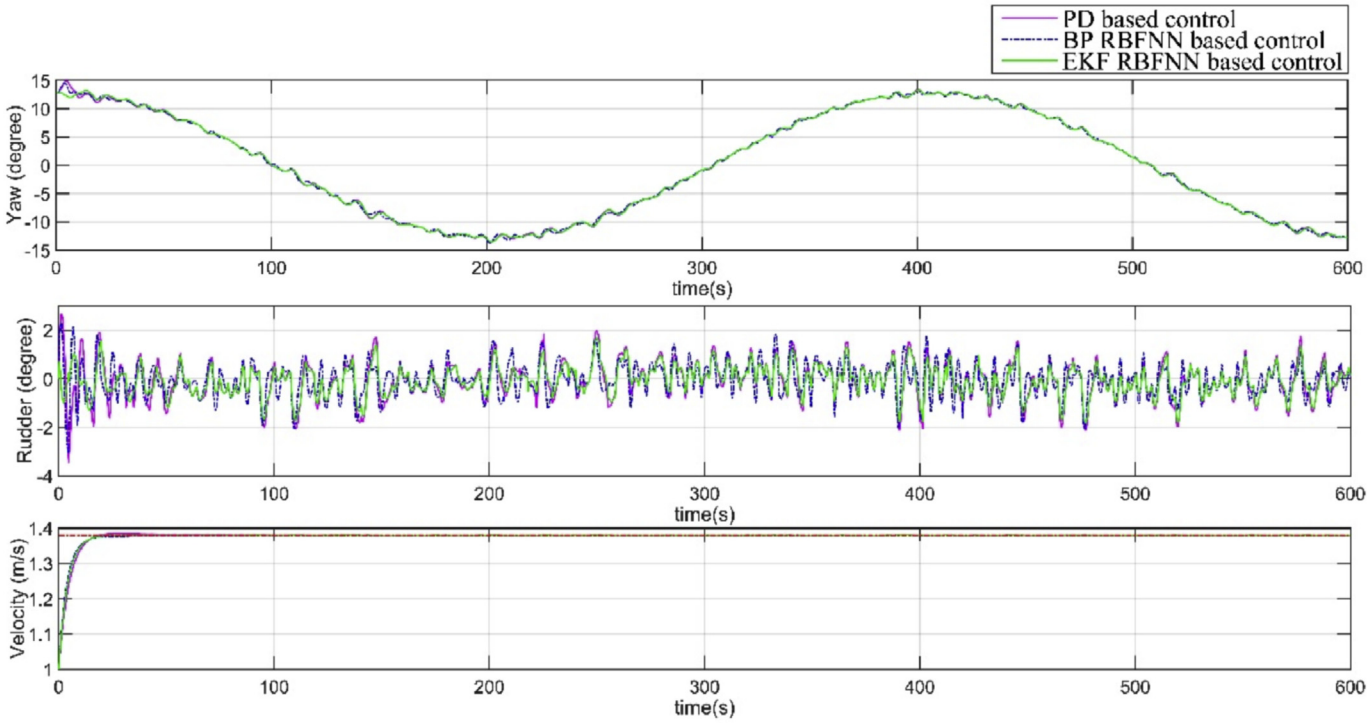

Fig. 7. The ship responses under the control of EKF RBFNN, BP RBFNN and PID controller based on the designed trajectory.

5. Experiment results and discussion

In order to mitigate the model-reality mismatch, the proposed control algorithm was applied to the realistic process experimentally. Normally, before the execution of control experiments, the raw measurements collected from low-cost sensors cannot be utilised directly because these measurements are easily affected by the distortion, declination, uncertain bias and coloured noises. Therefore, the signal conditioning and data filtering are required. In the experimental study, the signal conditioning and Kalman filters for yaw angle estimation were used and deployed in the experiment programme in LabVIEW. Based on the current observation and prediction states from the IMU readings, the most likely current heading angle of the vessel can be optimised (Wang et al., 2017c).

During the experiments, the approximate direction of the wind generated waves was approximately at 45 *degrees*, the speed of the south-west wind did not exceed 4 m/s, but the occasional wind was strong around the Trevallyn Lake. The experiment programs (see Fig. 8) were developed in LabVIEW, in which the data processing algorithms and the EKF RBFNN based controller were written in M-language using the Mathscript Node Module. In the controller, the initial weights $\boldsymbol{w}_0 = [\,-160 \quad -15 \quad 19 \quad -30 \quad -3 \quad 28 \quad -22 \quad 22210\,]$ validated in the simulations were utilised in case of mis-controlling, since using the random initial weights may lead to the uncontrollable and mis-converge in the initial phase. The FRMSS was fully loaded with propellers shaft at 900 *rpm*. The control law for rudder alternation was constrained within ±15 *degrees* and the maximum slew rate was limited within ±10 *degree*/*s*. Once the control program was deployed into the myRIO, the signal conditioning worked with the sampling rate at 10 *Hz* and the control algorithm also worked recursively with interval time at 0.1 s. Because of the insufficient accuracy of the low-cost GPS data and speed observation, the course keeping experimental tests were only reported in this study.

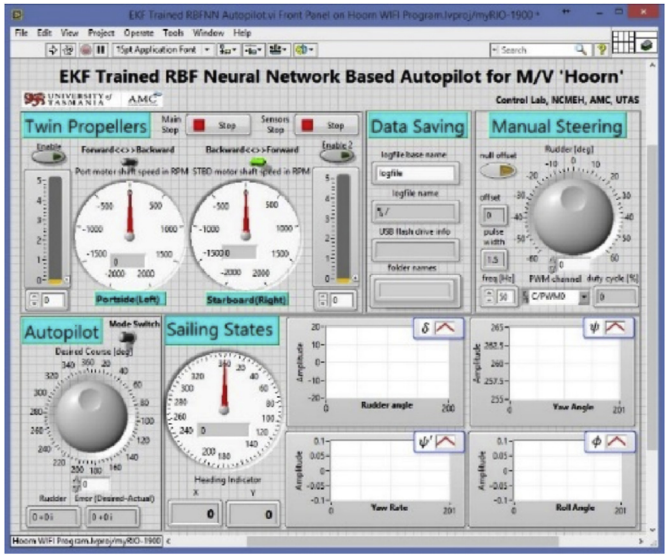

Fig. 8. The control panel of the host computer for remotely operating and monitoring 'Hoorn'.

The adopted courses are straight lines to guide the ship sailing forward, so the direction of the ship will stabilise on the corresponding yaw angle. To validate the control performance of the proposed autopilot, two experiment scenarios with courses at 225° and 255° were implemented (see Fig. 9). The parameters in the EKF training algorithms and RBFNN architectures consisted with that in the simulations. As the communication range of the WIFI router is about 100 m, experiment results in 100 s are reported.

The first set of experiments were conducted nearby the jetty with the desired course at 225°. The performances of the proposed control systems are illustrated in Fig. 10; while the cost values of yaw error and rudder actions as well as the corresponding maximum deviations are outlined in Table 3. The results indicate that the EKF RBFNN based controller has successfully made the FRMSS converge on the desired course smoothly. Although the BP RBFNN based controller and PD based controller also maintain the ship sailing on the preferred course, the maximum deviations are larger than that of EKF RBFNN based controller. Meanwhile, the EKF RBFNN based controller has lower rudder action costs in comparison with the BP RBFNN and PD based control system.

The second set of experiments were conducted nearby a cape with the desired course angle at 255°. The disturbances of waves are larger than that of the previous experiment site. The experiments results in Fig. 11 and Table 4 indicate that the EKF RBFNN based controller has the highest precision in course keeping among the three types of control systems. Although the increased external disturbance leads to the large rudder actions in compensating the environmental effects, the rudder actions of using EKF RBFNN autopilot are still more effective in comparison with that of the BP RBFNN and PD autopilot.

According to the above-mentioned experimental scenarios, the EKF RBFNN based controller has been verified to be capable of getting higher control accuracy and coping with the environmental disturbances with efficient rudder actions. The comparisons also demonstrated the superiority of the EKF based training method to the BP based training method in fast converging speed.

Fig. 9. Experiment under the control of EKF RBFNN based autopilot.

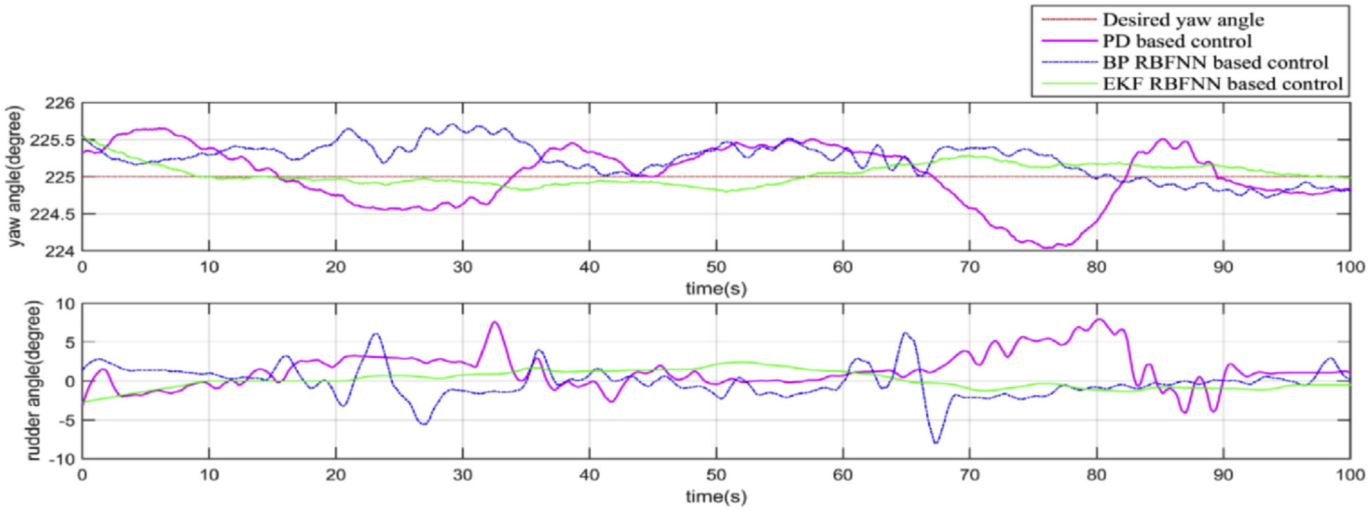

Fig. 10. Yaw angle and rudder action under the EKF RBFNN and BP RBFNN based control with desired course at 225°.

Table 3
The cost values and maximum values of yaw error and rudder action with yaw angle at 225°.

Controller	Yaw Error Cost	Maximum Yaw Error	Rudder Action Cost	Maximum Rudder Angle
PD	164.64	0.97	6923.75	7.9
BP RBFNN	107.54	0.71	3883.35	8.0
EKF RBFNN	21.21	0.53	1317.71	2.7

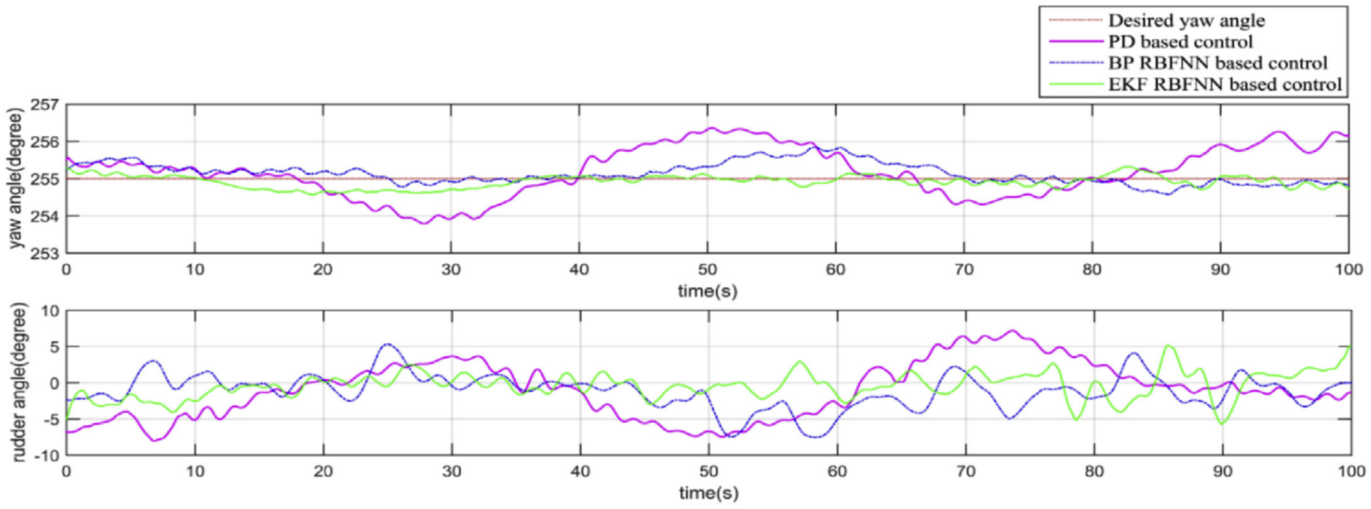

Fig. 11. Yaw angle and rudder action under the EKF RBFNN and BP RBFNN based control with desired course at 255°.

Table 4
The cost values and maximum values of yaw error and rudder action with yaw angle at 255°.

Controller	Yaw Error Cost	Maximum Yaw Error	Rudder Action Cost	Maximum Rudder Angle
PD	477.43	1.36	15,621.65	8.1
BP RBFNN	97.31	0.85	6806.92	7.5
EKF RBFNN	34.50	0.43	3379.35	5.7

6. Conclusion

In this study, the RBFNN based control system has been investigated to achieve the trajectory tracking of the ship with sailing uncertainties and unknown dynamics. The EKF based training algorithm has been proposed to improve the converge speed and avoid computationally expensive. The newly developed free running model scaled ship and the relevant mathematical model were adopted to verify the control performance of the proposed controller. The robustness of the developed autopilot has been

verified through analysing the motion responses of the ship advancing with random environmental disturbances and complex reference trajectory. In order to demonstrate the advantages of proposed EKF RBFNN based control system, the performance of the widely employed BP trained RBFNN control and conventional PD based control for the same tasks have been adopted for comparison. The experimental and numerical results have indicated that the EKF RBFNN based autopilot is feasible to accomplish the tasks of ship's motion control with small overshoot and short settling time. Simultaneously, the actions of rudder using EKF RBFNN based controller are smaller and smoother than that of the BP RBFNN based controller. In conclusion, the main advantages of the EKF RBFNN based control method consist in the rapid respond to the sailing uncertainties and complex underactuation, as well as the reasonable control actions.

From the view of commercial utilisation, the results indicate that low-cost intelligent autopilot can be achieved based on the control scheme executed on the current computing platform for marine vessels. In future studies, further investigation will concern the installation of the accurate positioning sensor to achieve trajectory tracking and other complicated manoeuvres experimentally. Also, remote communication technique with longer range will be adopted to extend the experiment time to further investigate the reliability of the control system. The study about the control of automatic berthing and underthing by using the rudder as well as the shaft speed difference of propellers will be investigated.

Acknowledgements

This research is funded by the Tasmanian Institutional Grants Scheme (IGS) and the Guangdong MEPP Fund (Grant No. GDOE 2019A18). The authors would like to appreciate Michael Underhill and Yufei Wang for the technical supply during the experiments.

Appendix. :Non-Dimensional Main Hydrodynamic and Manoeuvring Characteristics of the Ship “Hoorn”

References

Burns, R., 1995. The use of artificial neural networks for the intelligent optimal control of surface ships. IEEE J. Ocean. Eng. 20, 65–72.
Dai, S.-L., Wang, C., Luo, F., 2012. Identification and learning control of ocean surface ship using neural networks. IEEE Trans. Ind. Inform. 8, 801–810.
Dong, Z., Wan, L., Li, Y., Liu, T., Zhang, G., 2015. Trajectory tracking control of underactuated USV based on modified backstepping approach. Int. J. Naval Arch. Ocean Eng. 7, 817–832.
Fang, M.-C., Lee, Z.-Y., 2016. Application of neuro-fuzzy algorithm to portable dynamic positioning control system for ships. Int. J. Naval Arch. Ocean Eng. 8, 38–52.
Fang, M.C., Zhuo, Y.Z., Lee, Z.Y., 2010. The application of the self-tuning neural network PID controller on the ship roll reduction in random waves. Ocean Eng. 37, 529–538.
Fossen, T., 2011. Hydrostatics. *Handbook of Marine Craft Hydrodynamics and Motion Control*.
Fossen, T.I., 1994. Guidance and Control of Ocean Vehicles. John Wiley & Sons Inc.
Ge, S.S., Hang, C.C., Lee, T.H., Zhang, T., 2013. Stable Adaptive Neural Network Control. Springer Science & Business Media.
Liu, J., 2013. Radial Basis Function (RBF) Neural Network Control for Mechanical Systems: Design, Analysis and Matlab Simulation. Springer Berlin Heidelberg.
Morawski, L., Pomirski, J., 1998. Ship track-keeping: experiments with a physical tanker model. Contr. Eng. Pract. 6, 763–769.
Naeem, W., Sutton*, R., Chudley, J., Dalgleish, F., Tetlow, S., 2005. An online genetic algorithm based model predictive control autopilot design with experimental verification. Int. J. Contr. 78, 1076–1090.
Park, J., Sandberg, I.W., 1991. Universal approximation using radial-basis-function networks. Neural Comput. 3, 246–257.
Purushothaman, S., 2010. Tool wear monitoring using artificial neural network based on extended Kalman filter weight updation with transformed input patterns. J. Intell. Manuf. 21, 717–730.
Rigatos, G., Tzafestas, S., 2006. Adaptive fuzzy control for the ship steering problem. Mechatronics 16, 479–489.
Ruck, D.W., 1990. Characterization of Multilayer Perceptrons and Their Application to Multisensor Automatic Target Detection. AIR FORCE INST OF TECH WRIGHT-PATTERSON AFB OH SCHOOL OF ENGINEERING.
Sanchez, E.N., Alan S, A.Y., Loukianov, A.G., 2008. Discrete-time High Order Neural Control: Trained with Kalman Filtering. Springer Science & Business Media.
Sgobbo, J.N., Parsons, M.G., 1999. Rudder/fin roll stabilization of the USCG WMEC 901 class vessel. Mar. Technol. SNAME News 36, 157.
Sum, J., Leung, C.-S., Young, G.H., Kan, W.-K., 1999. On the Kalman filtering method in neural network training and pruning. *Neural Networks*. IEEE Trans. on 10, 161–166.
Sun, B., Zhu, D., Yang, S.X., 2014. A bioinspired filtered backstepping tracking control of 7000-m manned submarine vehicle. IEEE Trans. Ind. Electron. 61, 3682–3693.
Tannuri, E., Agostinho, A., Morishita, H., Moratelli, L., 2010. Dynamic positioning systems: an experimental analysis of sliding mode control. Contr. Eng. Pract. 18, 1121–1132.
Trebatick, P., 2005. Recurrent neural network training with the extended kalman

Table 5
Main Hydrodynamic Coefficients of The Free Running Model in the Degree of Surge, Sway, Yaw and Roll.

Category	Value	Category	Value
Sway	$Y_v' = -0.0549$ $Y_r' = -0.00129$ $Y_{vvv}' = 0.02394$ $Y_{vvr}' = -0.242$ $Y_{vrr}' = -0.1299$ $Y_{vv\phi}' = -0.0148$	Surge	$X_{uu}' = -0.0024$ $X_{vr}' = -0.0024$ $X_{vv}' = 0.0149$ $X_{rr}' = 0.0207$ $X_{\phi\phi}' = 0.0166$
Roll	$K_v' = 0.00089$ $K_r' = 0.00013$ $K_p' = 0.00006$ $K_{vvv}' = -0.0264$ $K_{vvr}' = -0.008$ $K_{vrr}' = 0.0096$ $K_{vv\phi}' = -0.0103$ $K_{rr\phi}' = -0.00159$	Yaw	$N_v' = -0.0095$ $N_r' = -0.0046$ $N_p' = -0.00008$ $N_{vvv}' = 0.0034$ $N_{rrr}' = 0.0017$ $N_{vvr}' = -0.0216$ $N_{vrr}' = 0.0011$ $N_{vv\phi}' = -0.0191$ $N_{v\phi\phi}' = -0.0058$ $N_{rr\phi}' = -0.0033$ $N_{r\phi\phi}' = 0.0024$

Table 6
Main Manoeuvring Characteristics of The Free Running Model Hoorn

Category	Value	Category	Value
Mass and Added Mass Moment of Inertial Interference Parameters	$m_0' = 0.0084$ $m_x' = 0.000315$ $m_y' = 0.0075$ $I_x' = 0.0000773$ $J_x' = 0.0000154$ $I_z' = 0.002$ $J_z' = 0.002$ $t_R' = 0.3825$ $a_H' = 0.237$	Dimension Parameters	$l_y' = 0.03$ $\alpha_y' = 0.05$ $l_x' = 0.031$ $\overline{H}' = 0.00354$ $z_R' = 0.033$ $x_R' = -0.5$ $x_H' = -0.45$

filter. In: IIT. SRC 2005: Student Research Conference, vol. 57.
Wang, N., Er, M.J., 2015. Self-constructing adaptive robust fuzzy neural tracking control of surface vehicles with uncertainties and unknown disturbances. IEEE Trans. Contr. Syst. Technol. 23, 991–1002.
Wang, N., Lv, S., Zhang, W., Liu, Z., Er, M.J., 2017a. Finite-time observer based accurate tracking control of a marine vehicle with complex unknowns. Ocean Eng. 145, 406–415.
Wang, N., Su, S.-F., Han, M., Chen, W.-H., 2018a. Backpropagating constraints-based trajectory tracking control of a quadrotor with constrained actuator dynamics and complex unknowns. IEEE Trans. Systems, Man, and Cybernetics: Syst. 1–16.
Wang, N., Su, S.-F., Pan, X., Yu, X., Xie, G., 2018. Yaw-guided trajectory tracking control of an asymmetric underactuated surface vehicle. IEEE Trans. Ind. Inform. 15 (6), 3502–3513.
Wang, N., Sun, J.-C., Han, M., Zheng, Z., Er, M.J., 2018c. Adaptive approximation-based regulation control for a class of uncertain nonlinear systems without feedback linearizability. IEEE Trans. Neural Netw. Learn. Syst. 29, 3747–3760.
Wang, Y., Chai, S., Nguyen, H.D., 2017b. Modelling of a surface vessel from free running test using low cost sensors. In: Control, Automation and Robotics (ICCAR), 2017 3rd International Conference on. IEEE, pp. 299–303.
Wang, Y., Nguyen, H.D., Chai, S., Khan, F., 2015. Radial basis function neural network based rudder roll stabilization for ship sailing in waves. In: Control Conference (AUCC), 2015 5th Australian. IEEE, pp. 158–163.
Wang, Y., Shuhong, C., Nguyen, H.D., 2017c. Modelling of a surface vessel from free running test using low cost sensors. In: 2017 3rd International Conference on Control, Automation and Robotics (ICCAR), 24-26 April 2017, pp. 299–303.
Wu, J., Peng, H., Ohtsu, K., Kitagawa, G., Itoh, T., 2012. Ship's tracking control based on nonlinear time series model. Appl. Ocean Res. 36, 1–11.
Yahui, L., Sheng, Q., Xianyi, Z., Okyay, K., 2004. Robust and adaptive backstepping control for nonlinear systems using RBF neural networks. IEEE Trans. Neural Network. 15, 693–701.
Yang, H., Li, J., Ding, F., 2007. A neural network learning algorithm of chemical process modeling based on the extended Kalman filter. Neurocomputing 70, 625–632.